A comparison of the Bidomain and the adapted monodomain models in electro-cardiology

Charles Pierre, Yves Bourgault

A COMPARISON OF THE BIDOMAIN AND THE ADAPTED MONODOMAIN MODELS IN ELECTRO-CARDIOLOGY

CHARLES PIERRE AND YVES BOURGAULT

Abstract. In this paper we compare two commonly used models in electro-cardiology: the bidomain and the (adapted) monodomain models. These models are used to simulate spreading of excitation and recovery in myocardial tissues including anisotropic conduction due to muscular fiber rotations. The comparison is held numerically considering the activation time mappings predicted by the two models. Two test cases are considered: firstly a two-dimensional academic test case and secondly a realistic setting involving a complex geometry of the ventricles based on a medical image segmentation and rotating anisotropy. To distinguish between the error induced by the discretisation and the discrepancy between the models, a convergence numerical study is made. From these numerical studies two facts are drawn: the discrepancy between the two models is quite small (of order or below 1%) and smaller than the discretisation error for commonly ran simulations in biomedical engineering.

1. Introduction

The bidomain model [23, 14, 1, 9, 24] is currently considered as the most accurate and physiologically founded description for the electrical cardiac behaviour and is widely used to simulate action potential speeding in the myocardium as well as electrocardiograms. Its mathematical formulation reads a system of two parabolic reaction diffusion equations, or equivalently one parabolic reaction diffusion equation coupled with one elliptic equation. This system is coupled with an ODE system describing cell membrane kinetics. The mathematical properties of the bidomain model are quite delicate: it has been shown in [3] that it can be reformulated into one parabolic semi-linear PDE but including non locality in space. These structural properties bring numerical

Date: December 13, 2010.

Key words and phrases. Electro-cardiology, bidomain and monodomain models, excitation process and activation time, reaction diffusion equations, numerical simulations, anisotropic diffusion.

difficulties. One ill-conditioned linear system inversion is required per time step. Moreover cardiac action potential involving fast space and time potential variations, fine space and time grids must be considered. For these two reasons simulating the cardiac electrical activity with the bidomain model has a very high cost, and many efforts towards the reduction of this cost have been made, e.g. [7, 11, 6]. The monodomain model is a simplification of the bidomain model reading a single parabolic reaction diffusion equation (still coupled with the same ODE system modelling cell membrane). Although this simplification has no mathematical general justification, and although the monodomain model lacks physiological foundation, it is commonly used in electro-cardiology: firstly because it obviously lead to much lower computational efforts than the bidomain model (as analyzed in [22]). The second reason motivating the interest for the monodomain model is that, as an approximation of the bidomain model, it may serve to improve numerical scheme efficiency for the bidomain model [13] or to build powerful preconditioners [12, 12]. The quality of the monodomain model approximation cam moreover be numerically optimized as developed in [17]

In comparison with the amount of papers dealing with the bidomain and the monodomain models, quite few studies measuring the discrepancy between these two models are available. In [8, 19], a precise approximation of the bidomain model, namely the adapted or modified monodomain model, is stated and compared with the bidomain model. In [8], Colli-Franzone et al. compared the two models on an academic 3D test case, a small slab of cardiac tissue, including anisotropy (orthotropic or axysymmetric). Their comparison is based on activation time, recovery time and action potential duration measurements. They observed a strong qualitative agreement between the two models and a noticeable quantitative difference (5 to 10 % of relative error on the activation time e.g.). In [19], Potse et al. compared the two models on a complete 3D human hear. The discrepancy between the models is here reported to be small but not precisely measured (in terms of activation time, recovery time and epicardial potential measurements). Although a strong quantitative agreement for the epicardial potential depicted in the paper is clear, quantitative differences are again visible.

One problem raised with these two papers is: what is the amount of error really due to the change of model and what is the error due to discretisation ? Although fine meshes have been considered (the mesh size Δx is of 0.1 mm in [8] and of 0.2 mm in [19]) it is not clear whether this resolution is sufficiently small to dissipate discretisation error from the results. Discretisation error are even pointed out in [19]:

potential wave velocities are measured on two meshes of 0.1 and 0.2 mm resolution for both models. The discretisation errors are of order 5% and 20% for the velocities along and transversally to the muscular fibres respectively. This illustrate that even on very fine meshes the discretisation error might be as high as the model discrepancy.

In this paper we address the question of the discrepancy between the two models *at the continuous level*. The error criterion is the activation time. To get rid of the discretisation error, a convergence study is made: using series of successively refined meshes. Two different test cases are considered in dimension 2: an academic test case on the unit square including constant anisotropy and a realistic second test case on a slice of the two ventricles obtained via medical image segmentation and including rotating anisotropy. For both test cases the Luo and Rudy class II model of cell membrane [16] (for mammalian ventricular cells) will be considered.

The paper is organized as follows. The bidomain and the adapted monodomain models are formulated in Sec. 2. In Sec. 3 the numerical implementation of the models is described as well as the two tests cases. The simulation results are given in Sec. 4, conclusions are drawn in Sec. 5.

2. Models

The heart of a living organism is assumed to occupy a fixed domain Ω that is a bounded open subset of $\mathbb{R}^d$, $d = 2, 3$. At the macroscopic scale the cardiac tissue is considered as the superimposed of the intra-cellular *(i)* and extra-cellular *(e)* media. The *bidomain* and *adapted monodomain* models presented here describe the heart electrical activity at this scale. For a derivation of the bidomain model from physiological considerations at the microscopic scale we refer to [23, 14, 1, 9, 24].

These two models involve two electrical potentials: the *intra-* and *extra-cellular potentials* $u_i,\ u_e :\ Q \mapsto \mathbb{R}$, where Q denotes the time-space cylinder $(0, T) \times \Omega$. Their difference is referred to as the *transmembrane potential*: $v := u_i - u_e\ :\ Q \mapsto \mathbb{R}$. The heart tissue has a fibrous organization into muscular fibres. This causes anisotropy for the electrical conductivity described by two conductivity tensors $\sigma_i(x)$ and $\sigma_e(x)$ at point $x \in \Omega$. Introducing the conductivities $g^l_{i,e}$, $g^t_{i,e}$ longitudinal and transverse to the fibres, these tensors read:

$$\sigma_i(x) = \mathrm{Diag}(g^l_i, g^t_i), \quad \sigma_e(x) = \mathrm{Diag}(g^l_e, g^t_e), \tag{1}$$

in a moving system of coordinates whose principal direction is given by the fibre orientation at point x. The fibres are moreover assumed to be tangent to the heart boundary $\partial\Omega$.

In this paper, we consider the case of an isolated heart (the interaction with the surrounding tissues is neglected). This insulation assumption reads a zero flux boundary condition on u_i and u_e physically meaning that no current flows out of the heart. Because of the tangency of the fibres along $\partial\Omega$, this condition is equivalent with:

$$\nabla u_i \cdot \mathbf{n} = \nabla u_e \cdot \mathbf{n} = 0 \quad \text{on} \quad \partial\Omega, \tag{2}$$

$$\text{and so,} \qquad \nabla v \cdot \mathbf{n} = 0 \quad \text{on} \quad \partial\Omega. \tag{3}$$

2.1. **Bidomain model.** The bidomain model reads the three following equations, for $(t,x) \in Q$:

$$\begin{cases} \operatorname{div}((\sigma_i(x) + \sigma_e(x))\nabla u_e) = -\operatorname{div}(\sigma_i(x)\nabla v), \\ \chi\left(c\partial_t v + I_{ion}(v,\mathbf{w}) - I_{st}(t,x)\right) = \operatorname{div}(\sigma_i(x)\nabla(u_e+v)), \\ \partial_t \mathbf{w} = g(v,\mathbf{w}). \end{cases} \tag{4}$$

In equation 2, c denotes the membrane surface capacitance, χ is the rate of cell membrane surface per unit volume (homogenization parameter), $I_{st} : Q \mapsto \mathbb{R}$ is the stimulation current (source term). $I_{ion}(v,\mathbf{w})$ (reaction term) denotes the surface ionic current distribution on the membrane: its evolution is controlled by the gating variable $\mathbf{w} : Q \mapsto \mathbb{R}^N$ via the ODE system in line 3. The definitions of I_{ion} and of g are fixed by the chosen ionic model in 2.4.
Equations in (4) are closed by the boundary condition (2) and by an initial datum imposed on v and $\mathbf{w}$:

$$v(0,x) = v_0(x), \quad \mathbf{w}(0,x) = \mathbf{w}_0(x), \quad x \in \Omega. \tag{5}$$

Clearly, the bidomain model equations (4), (2) and (5) are invariant under the simultaneous change of $u_e,$, u_i into $ue + k$, $u_i + k$ for $k \in \mathbb{R}$: we therefore impose the normalization condition

$$\int_\Omega u_e(t,\cdot)dx = 0. \tag{6}$$

2.2. **Adapted monodomain model.** The adapted monodomain model is a simplification of the bidomain model where the transmembrane potential is simply defined by a parabolic reaction-diffusion equation, for $(t,x) \in Q$:

$$\begin{cases} \chi\left(c\partial_t v + I_{ion}(v,\mathbf{w}) - I_{st}(t,x)\right) = \operatorname{div}(\sigma_m(x)\nabla v), \\ \partial_t \mathbf{w} = g(v,\mathbf{w}), \end{cases} \tag{7}$$

with boundary condition (3) and initial condition (5). The conductivity tensor σ_m is defined as the harmonic mean between σ_i and σ_e,

$$\sigma_m^{-1}(x) := \sigma_i^{-1}(x) + \sigma_e^{-1}(x). \tag{8}$$

Again, the tangency of the fibres to the domain boundary implies that $\sigma_m(x)\mathbf{n}$ and $\mathbf{n}$ have the same direction on $\partial\Omega$, so that (3) precisely is the classical homogeneous Neumann boundary condition on $\partial\Omega$ associated with the operator $\mathrm{div}(\sigma_m\nabla\cdot)$.

The potential $v : \ Q \mapsto \mathbb{R}$ being defined by equations (7) (3) (5), u_e can be recovered using the second equation in (4), this will not be discussed here.

2.3. **Comments.** In the adapted monodomain model framework, v is independent from u_e; whereas for the bidomain model, v and u_e are strongly coupled and in general none of these two quantities can be computed independently from the other one. This illustrates a complete difference of nature between these two models which we briefly discuss here.

In [3] it has been showed that the bidomain model can be reformulated in terms of v only as follows:

$$\chi\left(c\partial_t v + I_{ion}(v,\mathbf{w}) - I_{st}(t,x)\right) = \mathcal{A}v, \quad \partial_t\mathbf{w} = g(v,\mathbf{w}),$$

where $\mathcal{A}$ denotes the harmonic mean between the two elliptic operators $\mathrm{div}(\sigma_i\nabla\cdot)$ and $\mathrm{div}(\sigma_e\nabla\cdot)$. This operator is non-local in general, in the following sense: $\mathcal{A}u(x)$ is not determined by the values of u in a neighbourhood of the point x. Precisely, the definition of $\mathcal{A}u$ requires an elliptic problem inversion. The strong coupling between v and u_e precisely relies on this fact. However, in some particular cases (in dimension 1 or in case of *equal anisotropy ratio*, i.e. if $\sigma_e(x) = k\ \sigma_i(x)$ for $k \in \mathbb{R}$) one has the equality $\mathcal{A} = \mathrm{div}(\sigma_m\nabla\cdot)$: *i. e.* the two models here coincide.

These cases are exceptional. In general $\mathcal{A}$ is non local and the two models do not match. The adapted monodomain model thus is based on the heuristic approximation $\mathcal{A} \simeq \mathrm{div}(\sigma_m\nabla\cdot)$. Its motivation is to benefit from the numerical facilities provided by this approximation. On the contrary of the bidomain model, no physiological interpretation for (7) has to be sought.

We point out that the equal anisotropy ratio condition do not fit with the experimental data. The conductivities considered in this paper (introduced in the following subsection and given in Tab. 1) induce anisotropy ratios between the longitudinal and transverse directions of 9.0 and 2.0 for the intra and extra-cellular medias respectively.

2.4. **Model settings.** In (4) and (7), the reaction terms I_{ion} and g are fixed by choosing an ionic model: such a model describes the ion transfer across the cell membrane due to the cell metabolism. The gating variable $\mathbf{w}$ being here aimed to characterise the state of the cell membrane. We consider in this paper the Luo and Rudy II model [16] that has been developed for mammalian ventricular cells.

We shall use in this papers the parameters in Tab. 1. Cardiac tissue conductivities as well as χ are values subject to strong individual variabilities [5, 21]. A range for χ of 1500-2000 cm^{-1} seems suitable. Conductivities are taken from [15]. They induce an axial/transverse velocity ratio of 2.6. Setting χ to 1800 , axial and transverse velocities are of 0.5 and 0.19 m/s respectively, which data are in agreement with [21].

3. Methods

3.1. **Test case 1.** The following academic test case is considered. The domain Ω is set to $[0,1]^2$, a series of 6 meshes (from 177 to 160 000 nodes) is considered. Space and time steps being divided by two from level n to level $n+1$. On this geometry spreading of excitation potential waves is stimulated as depicted on Fig. 2. Excitation is initiated by applying a centered stimulation during a short period of time, precisely: $I_{st}(x,t) = 52\ \mu A$ for $5 < t < 5.1$ and $|x - x_0| < 0.1$ (x_0 denoting the centre of Ω) and $I_{st}(x,t) = 0$ otherwise. Initial condition (5) is taken as the rest state for the ionic model: $I_{ion}(v_0, \mathbf{w}_0) = 0 = g(v_0, \mathbf{w}_0)$. The domain Ω is assumed to be composed of a bundle of parallel horizontal muscular fibres, the following homogeneous tensors are defined:

$$\sigma_i(x) = \sigma_i := \mathrm{Diag}(g_i^l, g_i^t)\ , \quad \sigma_e(x) = \sigma_e := \mathrm{Diag}(g_e^l, g_e^t)\ . \tag{9}$$

3.2. **Test case 2.** We now consider a realistic 2D settings depicted on Fig. 1. The geometry has been obtained from the segmentation of a medical image of a human heart [20]: it represents a horizontal slice of the two ventricles with a resolution of 0.3 mm. Four meshes of this geometry have been built: from 143 000 to 1 257 000 nodes. Anisotropy is given from the fibrous organisation of the tissue following (1). A set of fibres rotating around the two ventricles and remaining tangent to the boundary has been built. Stimulation is initiated at 4 places (two on each ventricle) on the endocardium. A stimulation current of 52 μA is applied during 0.1 ms at these locations at time 20 ms and 25 ms on the left ventricle and right ventricle respectively.

3.3. **Implementation.** The following weak formulation of the bidomain model is considered, $\forall \psi \in H^1(\Omega)$:

(10)
$$\int_\Omega (\sigma_i + \sigma_e)\nabla u_e \cdot \nabla \psi dx + \int_\Omega \sigma_i \nabla v \cdot \nabla \psi dx = 0,$$

(11)
$$\chi c \partial_t \int_\Omega v\psi dx + \chi \int_\Omega (I_{ion}(v, \mathbf{w}) - I_{st}(x,t))\psi dx = \int_\Omega \sigma_i \nabla(u_e + v) \cdot \nabla \psi dx.$$

To this system is added the normalisation condition (6) to ensure uniqueness on u_e.

This formulation is discretised in time using an Euler semi-implicit scheme: implicit for the diffusion and explicit for the reaction. Spatial discretisation has been led using Control Volumes Finite Elements (CVFE, see eg [4]). One large linear system (symmetric and non-negative) has to be inverted at each time step. These inversions are the main numerical difficulty for the bidomain model: precise details on the implementation, and on the preconditioning of the bidomain model are available in [18].

The adapted monodomain model implementation is much simpler. We consider the classical weak formulation of the parabolic equation (7). It is discretised as for the bidomain model: using an Euler semi-implicit scheme in time and a CVFE discretisation in space.

Remark 1. *We eventually discuss the choice of the spatial discretisation. We numerically experimented that the result quality is highly sensitive to this choice. We compared 3 methods of order 2 for the elliptic problem discretisation: P1 finite element, Discrete Duality Finite Volumes (DDFV, see eg* [10, 2] *as applied to the bidomain model) and Control Volumes Finite Elements (CVFE, see eg* [4]*). The CVFE method gave the best results and will be used here.*
For the CVFE method the nodes are located at the mesh vertices, allowing to associate to the numerical solution a P1 function on the mesh elements, which property will be useful in the next subsection

3.4. **Numerical test.** One searches to measure the discrepancy between the bidomain and the adapted monodomain model at the continuous level. For this one needs to get rid of the errors caused by the discretisatrion. We proceed as follows:

- Firstly, we numerically study the convergence of the numerical schemes for both the bidomain and the adapted monodomain

models, using series of successively refined meshes. An a posteriori error estimate then allows to evaluate the error induced by discretisation.
- Secondly, the error between the (discrete) bidomain and adapted monodomain models is computed on each mesh. Once this error becomes wider than the discretisation errors measured in step one, one can deduce the discrepancy between the (continuous) bidomain and adapted monodomain models.

Because of its particular physiological importance, we adopt an error criterion based on the activation time. Activation time $\phi : \Omega \mapsto \mathbb{R}$ is defined at each point x as the time $\phi(x)$ such that $v(\phi(x), x) = v_s$ for a threshold value v_s set here to $-20\ mV$. The value $\phi(x)$ tells us at what time the excitation wave reaches the point x. Activation time for test cases 1 and 2 are depicted on Figs. 2 and 3 respectively.

Let us denote by $\mathfrak{T}_n$ the series of meshes. We consider the numerical activation time ϕ_n computed relatively to $\mathfrak{T}_m$. We compare ϕ_n and ϕ_{n+1} by introducing the projection $\tilde{\phi}_n$ of ϕ_n on the finer level $\mathfrak{T}_{n+1}$. For this ϕ_n is considered as a P1 function (i.e. continuous piecewise affine) on the elements of $\mathfrak{T}_n$. The values of this function are computed on the vertices of $\mathfrak{T}_{n+1}$, which data allows to define the considered projection $\tilde{\phi}_n$ as a P1 function on the elements of $\mathfrak{T}_{n+1}$. The following error is computed:

$$e_2^n := \|\tilde{\phi}_n - \phi_{n-1}\|_{L^2(\Omega)} \quad , \quad r_2^n := \frac{e_2^{n-1}}{e_2^n}. \tag{12}$$

We define the discrepancy between the bidomain and adapted monodomain models as:

$$\delta_2^n := \frac{\|\phi_n^b - \phi_n^m\|_{L^2(\Omega)}}{\|\phi_n^b\|_{L^2(\Omega)}}, \tag{13}$$

where b and m stands for bidomain and adapted monodomain respectively.

4. Results

Test case 1. Numerical results on the convergence of the activation time are displayed in Tab. 2 and Tab. 3 for the bidomain and adapted monodomain models respectively. In both cases assuming an order 2 convergence with respect to the mesh size Δx seems reasonable.
Let us denote by ϕ_∞ the activation time for the continuous problem.

Following (rough) estimate,

$$\begin{aligned}\|\phi_n - \phi_\infty\|_{L^2(\Omega)} &\leq \|\phi_n - \phi_{n+1}\|_{L^2(\Omega)} + \|\phi_{n+1} - \phi_{n+2}\|_{L^2(\Omega)} + \dots \\ &\leq \frac{1/4}{1-1/4}\|\phi_n - \phi_{n-1}\|_{L^2(\Omega)}.\end{aligned}$$

We introduce a relative error estimator ε_2^n as:

$$\varepsilon_2^n := \frac{1}{3}\frac{e_2^n}{\|\phi_6\|_{L^2(\Omega)}}. \tag{14}$$

which estimator will be considered as an upper bound on $\|\phi_n - \phi_\infty\|_{L^2(\Omega)}/\|\phi_\infty\|_{L^2(\Omega)}$. Numerical results on ε_2^n are given in Tab. 4. These results illustrate that to obtain a good approximation of ϕ_∞ necessitates to consider really fine meshes: for an approximation of order 1% a space resolution of order 0.05 mm is needed.

The discrepancy δ_2^n between the (discrete) bidomain and adapted monodomain models is quantified in Tab. 5. Comparing these figures with Tab 4, one can see that for the finest mesh the discrepancy between the two models is higher than the discretisation errors with a factor 10. Thus the discrepancy between the bidomain and the adapted monodomain models appears of order 1%. Moreover one can infer from the figures in Tab. 5 a convergence of δ_2^n of order 3/2 with respect to the number of nodes. From this constatation one concludes to a discrepancy of 0.7 % $\pm$ 0.1%. It is remarkable that this estimate seems to be independent with the value of χ.

Test case 2. Convergence of both models is harder to observe in such a precise way as in test case 1 here. This is caused by the complexity of the model: the numerical geometry (the union of all triangles of one mesh) is not constant but simply converging towards the segmented heart domain. More precisely, the numerical results obtained showed that the discretisation error on the finest mesh is less than 3% for both models. This discretisation error is here 2 or 3 times higher than for test case one when comparing at equal mesh size.

The discrepancy δ_2^n between the (discrete) bidomain and adapted monodomain models has been computed and is given in Tab. 6. The figures are coherent enough to postulate a a discrepancy of roughly 1% that is moreover coherent with the results of test case 1.

5. Conclusion

The activation time computed with the bidomain and the adapted monodomain models were compared using firstly a two-dimensional academic test case and secondly a realistic setting involving a complex

geometry of the ventricles and rotating anisotropy. We draw the following two conclusions from this numerical study.

Firstly the discrepancy between the (continuous) bidomain and adapted monodomain models is quite small: in terms of relative error on the activation time, it is of order 1% for test case 2 and even smaller for test case 1. For the authors, Such a range of error is negligible for a field (biological sciences) where the tolerance on the data errors is much larger. It is also interesting to notice that this discrepancy (or rather its numerical approximation at first order) seems to be independent from the scaling parameter χ.

Secondly, the convergence study we made shows that the amount of error induced by the discretisation is high even on quite fine meshes. As expected, the higher χ, the larger this error. Using a realistic value for χ in computations ($\chi \in [1500, 2000]$) necessitates to use very fine meshes. The comparison between the two test cases moreover shows that this discretisation error is increased when considering complex geometries and non constant anisotropy.

As a result it appears that for usually ran simulations in biomedical engineering, the amount of error induced by the discretisation shall be higher than the real discrepancy between the models.

References

[1] L. Ambrosio, P. Colli-Franzone, and G. Savaré. On the asymptotic behaviour of anisotropic energies arising in the cardiac bidomain model. *Interfaces Free Bound.*, 2(3):213–266, 2000.

[2] B. Andreianov, M. Bendahmane, K. H.. Karlsen, and C. Pierre. Convergence of DDFV schemes for the bidomain cardiac model. *HAL Preprint*, 2010.

[3] Y. Bourgault, Y. Coudière, and C. Pierre. Existence and uniqueness of the solution for the bidomain model used in cardiac electrophysiology. *Nonlinear Analysis: Real World Applications*, 10(1):458–482, 2009.

[4] Z. Cai, J. Mandel, and S. McCormick. The finite volume element method for diffusion equations on general triangulations. *SIAM J. Numer. Anal.*, 28:392–403, 1991.

[5] L. Clerc. Directional differences of impulse spread in trabecular muscle from mammalian heart. *J. Physio.*, 255(2):335–346, 1976.

[6] P. Colli Franzone, P. Deuflhard, B. Erdmann, J. Lang, and L. F. Pavarino. Adaptivity in space and time for reaction-diffusion systems in electrocardiology. *SIAM J. Sci. Comput.*, 28(3):942–962 (electronic), 2006.

[7] P. Colli Franzone and L.F. Pavarino. A parallel solver for reaction-diffusion systems in computational electrocardiology. *Math. Models Methods Appl. Sci.*, 14(6):883–911, 2004.

[8] P. Colli-Franzone, L.F. Pavarino, and B. Taccardi. Simulating patterns of excitation, repolarization and action potential duration with cardiac Bidomain and Monodomain models. *Math. Biosci.*, 197(1):35–66, 2005.

[9] P. Colli-Franzone and G. Savaré. Degenerate evolution systems modeling the cardiac electric field at micro- and macroscopic level. *Evolution equations, semigroups and functional analysis*, 2002.

[10] Y. Coudiere, C. Pierre, O. Rousseau, and R. Turpault. 2D/3D DDFV scheme for anisotropic- heterogeneous elliptic equations, application to electrograms simulation from medical data. *Int. J. Finite Volumes*, 2009.

[11] M. Ethier and Y. Bourgault. Semi-implicit time discretization schemes for the bidomain model. *SIAM Journal of Numerical Analysis*, 46(5):2443–2468, 2008.

[12] L. Gerardo-Giorda, L. Mirabella, F. Nobile, M. Perego, and A. Veneziani. A model-based block-triangular preconditioner for the bidomain system in electrocardiology. *J. Comput. Phys.*, 228(10):3625–3639, 2009.

[13] L. Gerardo-Giorda, M. Perego, and A. Veneziani. Optimized schwarz coupling of bidomain and monodomain models in electrocardiology. *M2AN*, 2010.

[14] W. Krassowska and J.C. Neu. Homogenization of syncytial tissues. *CRC Crit. Rev. Biomed. Eng.*, 21(2):137–199, 1993.

[15] P. Le Guyader, F. Trelles, and P. Savard. Extracellular measurement of anisotropic bidomain myocardial conductivities. I. theoretical analysis. *Annals Biomed. Eng.*, 29(10):862–877, 2001.

[16] C.H. Luo and Y. Rudy. A Dynamic Model of the Cardiac Ventricular Action Potential I. Simulations of Ionic Currents and Concentration Changes. *Circ. Res.*, 74:1071–1096, 1994.

[17] B.F. Nielsen, T.S. Ruud, G.T. Lines, and A. Tveito. Optimal monodomain approximations of the bidomain equations. *Applied Mathematics and Computation*, 184:276–290, 2007.

[18] C. Pierre. Preconditioning the coupled heart and torso bidomain model with an almost linear complexity. *HAL Preprint*, 2010.

[19] M. Potse, B. Dube, J. Richer, A. Vinet, and RM. Gulrajani. A comparison of monodomain and bidomain reaction-diffusion models for action potential propagation in the human heart. *IEEE Trans. Biomed. Eng.*, 53(12):2425–2435, 2006.

[20] O. Rousseau. Geometrical modeling of the heart. *PHD Thesis, University of Ottawa*, 2010.

[21] MS. Spach, JF. Heidlage, PC. Dolber, and RC. Barr. Extracellular Discontinuities in Cardiac Muscle Evidence for Capillary Effects on the Action Potential Foot . *Circ. Res.*, 83:1144–1164, 1998.

[22] J. Sundnes, B.F. Nielsen, K.A. Mardal, X. Cai, G.T. Lines, and A. Tveito. On the computational complexity of the bidomain and the monodomain models of electrophysiology. *Annals of Biomedical Engineering*, 34:1088–1097, 2006.

[23] L. Tung. A bidomain model for describing ischemic myocardial D-D properties. *Ph.D. thesis, M.I.T.*., 1978.

[24] M. Veneroni. Reaction-diffusion systems for the microscopic cellular model of the cardiac electric field. *Math. Methods Appl. Sci.*, 29(14):1631–1661, 2006.

	Value	**Unit**
Cell membrane surface-to-volume ratio	$\chi = 1000 - 2000$	$[\text{cm}^{-1}]$
Membrane surface capacitance	$c = 1.$	$[\mu\ \text{F/cm}^2]$
Longitudinal intra-cellular conductivity	$g_i^l = 1.741$	[mS/cm]
Transverse intra-cellular conductivity	$g_i^t = 0.1934$	[mS/cm]
Longitudinal extra-cellular conductivity	$g_e^l = 3.906$	[mS/cm]
Transverse extra-cellular conductivity	$g_e^t = 1.970$	[mS/cm]

TABLE 1. Bidomain and adapted monodomain models parameters

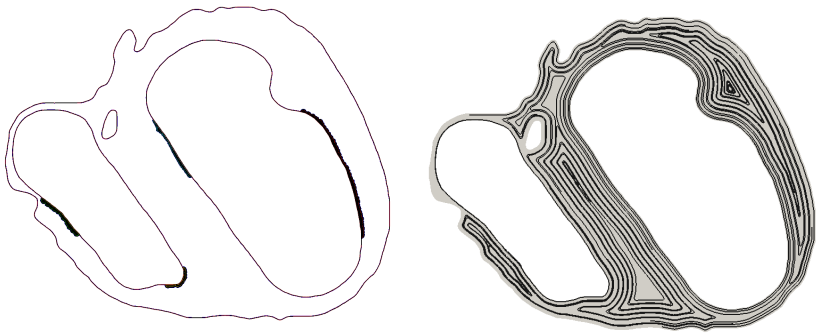

FIGURE 1. Test case 2 settings: stimulation sites location (above left) and fibrous structure of the tissue (above right).

# nodes	e_2^n	r_2^n	e_2^n	r_2^n	e_2^n	r_2^n
665	9.20		17.7		32.4	
2 577	2.82	3.3	4.79	3.7	6.91	4.7
10 142	0.851	3.3	1.53	3.1	2.29	3.0
40 257	0.151	5.6	0.300	5.1	0.490	4.7
160 385	$4.66\ 10^{-2}$	3.2	$6.89\ 10^{-2}$	4.4	$9.63\ 10^{-2}$	5.1

TABLE 2. Bidomain model: convergence of the activation time ϕ_n From left to right: $\chi = 1000$, 1500 and 2000 cm^{-1}.

APPENDIX A. FIGURES AND TABLES

(Charles Pierre)
LABORATOIRE DE MATHÉMATIQUES ET APPLICATIONS
UNIVERSITÉ DE PAU ET DU PAYS DE L'ADOUR
AV. DE L'UNIVERSITÉ BP 1155
64013 PAU CEDEX - FRANCE
E-mail address: charles.pierre@univ-pau.fr

DEPARTMENT OF MATHEMATIC AND STATISTICS, UNIVERSITY OF OTTAWA.
E-mail address: ybourg@uottawa.ca

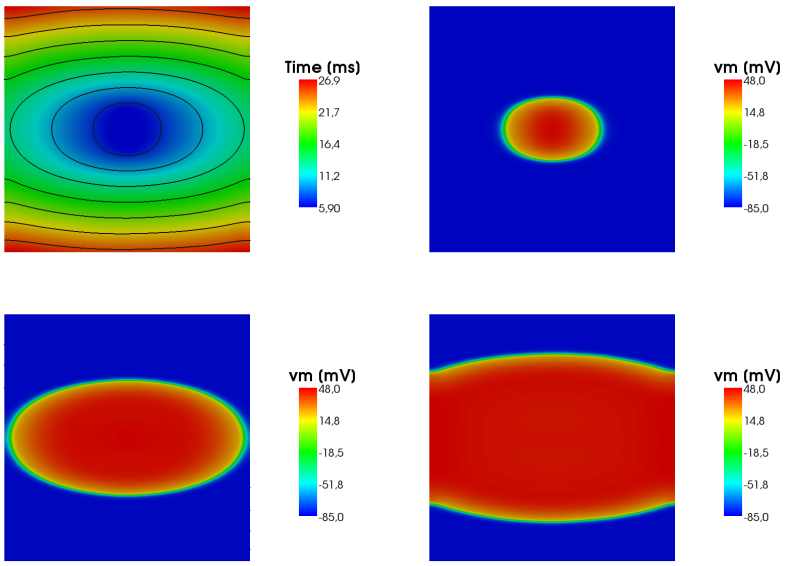

FIGURE 2. Activation time (above-left) and transmembrane potential wave spreading for the adapted monodomain model, $\chi = 1500$ on the finest mesh. The isolines (in black, above-left) are separated by 3 ms. Potential mappings are represented 3, 8 and 12 ms after the stimulation. Stimulation is initiated at time $t = 5$ ms.

# nodes	e_2^n	r_2^n	e_2^n	r_2^n	e_2^n	r_2^n
665	9.79		19.6		37.7	
2 577	3.04	3.2	5.15	3.8	7.44	5.1
10 142	0.949	3.2	1.68	3.1	2.49	3.0
40 257	0.198	4.8	0.314	4.5	0.590	4.2
160 385	3.7310^{-2}	5.3	6.9910^{-2}	5.4	0.111	5.3

TABLE 3. Adapted monodomain model: convergence of the activation time ϕ_n. From left to right: $\chi = 1000$, 1500 and 2000 cm^{-1}.

# nodes	ε_2^n	ε_2^n	ε_2^n
665	0.21	0.35	0.59
2 577	$6.3\ 10^{-2}$	$9.6\ 10^{-2}$	0.13
10 142	$1.9\ 10^{-2}$	$3.0\ 10^{-2}$	$4.2\ 10^{-2}$
40 257	$3.4\ 10^{-3}$	$6.0\ 10^{-3}$	$9.0\ 10^{-3}$
160 385	$1.0\ 10^{-3}$	$1.3\ 10^{-3}$	$1.8\ 10^{-3}$

ε_2^n	ε_2^n	ε_2^n
0.22	0.39	0.68
$6.8\ 10^{-2}$	0.10	0.13
$2.1\ 10^{-2}$	$3.3\ 10^{-2}$	$4.5\ 10^{-2}$
$4.4\ 10^{-3}$	$7.4\ 10^{-3}$	$1.1\ 10^{-2}$
$8.3\ 10^{-4}$	$1.4\ 10^{-3}$	$2.0\ 10^{-3}$

TABLE 4. Relative error estimation on ϕ_n for the bidomain model (left) and adapted monodomain model (right) for $\chi = 1000$, 1500, 2000 from left to right.

# nodes	δ_2^n	δ_2^n	δ_2^n
177	$4.18\ 10^{-2}$	$7.07\ 10^{-2}$	0.11
665	$2.87\ 10^{-2}$	$3.46\ 10^{-2}$	$3.95\ 10^{-2}$
2 577	$2.00\ 10^{-2}$	$2.42\ 10^{-2}$	$2.73\ 10^{-2}$
10 142	$1.47\ 10^{-2}$	$1.76\ 10^{-2}$	$1.99\ 10^{-2}$
40 257	$1.12\ 10^{-2}$	$1.33\ 10^{-2}$	$1.49\ 10^{-2}$
160 385	$9.59\ 10^{-3}$	$1.10\ 10^{-2}$	$1.20\ 10^{-2}$

TABLE 5. Discrepancy between the (discrete) bidomain and adapted monodomain models. From left to right: $\chi = 1000$, 1500 and 2000 cm^{-1}.

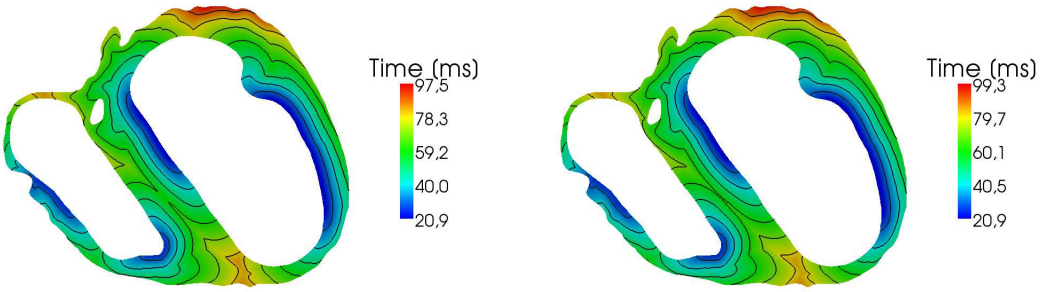

FIGURE 3. Test case 2. Activation time on the finest mesh (1 257 312 nodes) for the bidomain model (left) and the adapted monodomain model (right), isolines in black are separated by 10 ms, from 30 to 90 ms.

# nodes	δ_2^n
117 285	$1.94\ 10^{-2}$
279 447	$1.65\ 10^{-2}$
551 484	$1.50\ 10^{-2}$
1 110 270	$1.35\ 10^{-2}$

TABLE 6. Discrepancy between the (discrete) bidomain and adapted monodomain models on the heart slice geometry ($\chi = 1500\ cm^{-1}$).